20. H. P. Harding *et al.*, *Mol. Cell* **11**, 619–633 (2003).
21. D. Scheuner *et al.*, *Mol. Cell* **7**, 1165–1176 (2001).

ACKNOWLEDGMENTS

We thank D. J. Kwiatkowski and R. J. Kaufman for materials and M. Yuan, S. Breitkopf, J. J. Howell, M. Turner, and Y. Zhang for technical assistance. This research was supported by grants from the Bettencourt Foundation and LAM Foundation (I.B.-S.), TS Alliance (G.H.), NSF fellowship DGE-1144152 (S.J.H.R.), and NIH grants K99-CA194192 (I.B.-S.), P01-CA120964 (J.M.A. and B.D.M.), P30-CA006516 (J.M.A.), and R01-CA181390 and R35-CA197459 (B.D.M.). I.B.-S. and G.H. conceived, performed, and analyzed all experiments and prepared the manuscript. S.J.H.R performed the Cancer Genome Atlas analysis. J.M.A. performed LC-MS/MS experiments. B.D.M. directed research, reviewed all data, and prepared the manuscript. All authors reviewed the manuscript and declare no competing financial interests.

SUPPLEMENTARY MATERIALS

www.sciencemag.org/content/351/6274/728/suppl/DC1
Materials and Methods
Figs. S1 to S6
Tables S1 and 2
References (*22*, *23*)

17 July 2015; accepted 11 December 2015
10.1126/science.aad0489

BIOCHEMISTRY

Spatial colocalization and functional link of purinosomes with mitochondria

Jarrod B. French,[1]*† Sara A. Jones,[2]†‡ Huayun Deng,[3] Anthony M. Pedley,[4] Doory Kim,[2,6] Chung Yu Chan,[5] Haibei Hu,[3]§ Raymond J. Pugh,[4] Hong Zhao,[4] Youxin Zhang,[2] Tony Jun Huang,[5] Ye Fang,[3]* Xiaowei Zhuang,[2,6,7]* Stephen J. Benkovic[4]*

Purine biosynthetic enzymes organize into dynamic cellular bodies called purinosomes. Little is known about the spatiotemporal control of these structures. Using super-resolution microscopy, we demonstrated that purinosomes colocalized with mitochondria, and these results were supported by isolation of purinosome enzymes with mitochondria. Moreover, the number of purinosome-containing cells responded to dysregulation of mitochondrial function and metabolism. To explore the role of intracellular signaling, we performed a kinome screen using a label-free assay and found that mechanistic target of rapamycin (mTOR) influenced purinosome assembly. mTOR inhibition reduced purinosome-mitochondria colocalization and suppressed purinosome formation stimulated by mitochondria dysregulation. Collectively, our data suggest an mTOR-mediated link between purinosomes and mitochondria, and a general means by which mTOR regulates nucleotide metabolism by spatiotemporal control over protein association.

Purine levels in mammalian cells are maintained by the coordinated action of complementary salvage and de novo biosynthetic pathways. Whereas the salvage pathway maintains purine nucleotide levels under normal physiological conditions, the de novo pathway is up-regulated during growth (*1*, *2*) and altered in neoplastic cells (*3*, *4*). Purinosomes are mesoscale assemblies formed to protect unstable intermediates and increase metabolic flux through the de novo pathway (*5*–*9*). These structures are dynamic, form reversibly in response to purine depletion, and act to increase de novo purine biosynthesis (*5*, *6*, *10*). Their formation is cell cycle dependent and can be regulated by G protein–coupled receptor (GPCR) agonists and casein kinase 2 (*11*–*14*). An increased number of purinosome-containing cells correlates positively with the degree of purine salvage deficiency in Lesch-Nyhan disease (*15*). Cellular conditions resulting in disruption of purinosome formation led to enhanced sensitivity to cancer chemotherapeutics (*16*). An analogous cellular phenotype was also recently reported for a multifunctional protein involved in pyrimidine biosynthesis (*17*). These structures are examples of an increasing number of reported higher-order organizations involving metabolic proteins (*7*, *18*, *19*).

Considering that de novo purine biosynthesis not only provides the nucleotide precursors necessary for mitochondrial adenosine 5′-triphosphate (ATP) production but also conversely demands ATP for its operation, we hypothesized that a synergistic relationship between purinosomes and mitochondria might exist. This synergy would be even more critical in cells that preferentially use oxidative phosphorylation for ATP production, such as several cervical cancers, breast carcinoma, hepatoma, pancreatic cancer, and glioma cell lines (*20*, *21*). The relationship would also supply one-carbon units generated by the mitochondrial conversion of serine to formate for incorporation into the purine ring during de novo biosynthesis. In this work, we investigated the physical and functional relationship between purinosome and mitochondria using super-resolution imaging, a dynamic mass redistribution assay, and other biochemical measures.

Conventional fluorescence microscopy images initially suggested spatial proximity between purinosomes and mitochondria, but the high density of the mitochondrial network precluded clear demonstration and quantitative characterization of the colocalization between these two structures at diffraction-limited image resolution (fig. S1). To further investigate the spatial distribution of purinosomes, we used three-dimensional stochastic optical reconstruction microscopy (3D STORM), a super-resolution fluorescence imaging method (*22*–*24*), to image HeLa cells under conditions that promote the formation of purinosomes. Purinosomes were imaged via transient transfection of photoactivatable fluorescent protein (mEos2) (*25*) tagged formylglycinamidine ribonucleotide synthase (FGAMS or PFAS), a core purinosome component (*5*, *26*). Given the residual dimerization tendency of mEos2, we also tagged FGAMS to recently developed monomeric photoactivatable fluorescent protein, mMaple3 (*27*). The number and size distributions of purinosomes were independent of the tagging method (fig. S2).

To investigate purinosome-mitochondria colocalization, we induced purinosome formation by purine starvation, fixed the cells, and immunostained them for a mitochondrial outer membrane translocase (TOM20) using a photoswitchable fluorescent dye (Alexa Fluor 647). Two-color 3D STORM images of cells that exhibited purinosomes revealed spatial colocalization between purinosomes and mitochondria (Fig. 1). Under the conditions tested, a substantially larger fraction of purinosomes were colocalized with mitochondria than would be expected if the purinosomes were randomly distributed throughout the cytoplasm (Fig. 1G and fig. S3).

To provide further support for the potential physical interactions between purinosomes and mitochondria, we treated cells cultured in purine-depleted conditions with chemical cross-linkers, isolated the mitochondria, and compared the proteins present in these mitochondrial extracts

[1]Department of Biochemistry and Cell Biology, Department of Chemistry, Stony Brook University, Stony Brook, NY 11794, USA. [2]Department of Chemistry and Chemical Biology, Harvard University, Cambridge, MA 02138, USA. [3]Biochemical Technologies, Science and Technology Division, Corning Incorporated, Corning, NY 14831, USA. [4]Department of Chemistry, The Pennsylvania State University, University Park, PA 16802, USA. [5]Department of Engineering Science and Mechanics, The Pennsylvania State University, University Park, PA 16802, USA. [6]Howard Hughes Medical Institute, Harvard University, Cambridge, MA 02138, USA. [7]Department of Physics, Harvard University, Cambridge, MA 02138, USA.
***Corresponding author. E-mail: jarrod.french@stonybrook.edu (J.B.F.); fangy2@corning.com (Y.F.); zhuang@chemistry.harvard.edu (X.Z.); sjb1@psu.edu (S.J.B.)** †These authors contributed equally to this work. ‡Present address: The Broad Institute of MIT and Harvard, Cambridge, MA 02142, USA. §Present address: Medical Laboratory Science, Jefferson College of Health Science, Roanoke, VA 24013, USA.

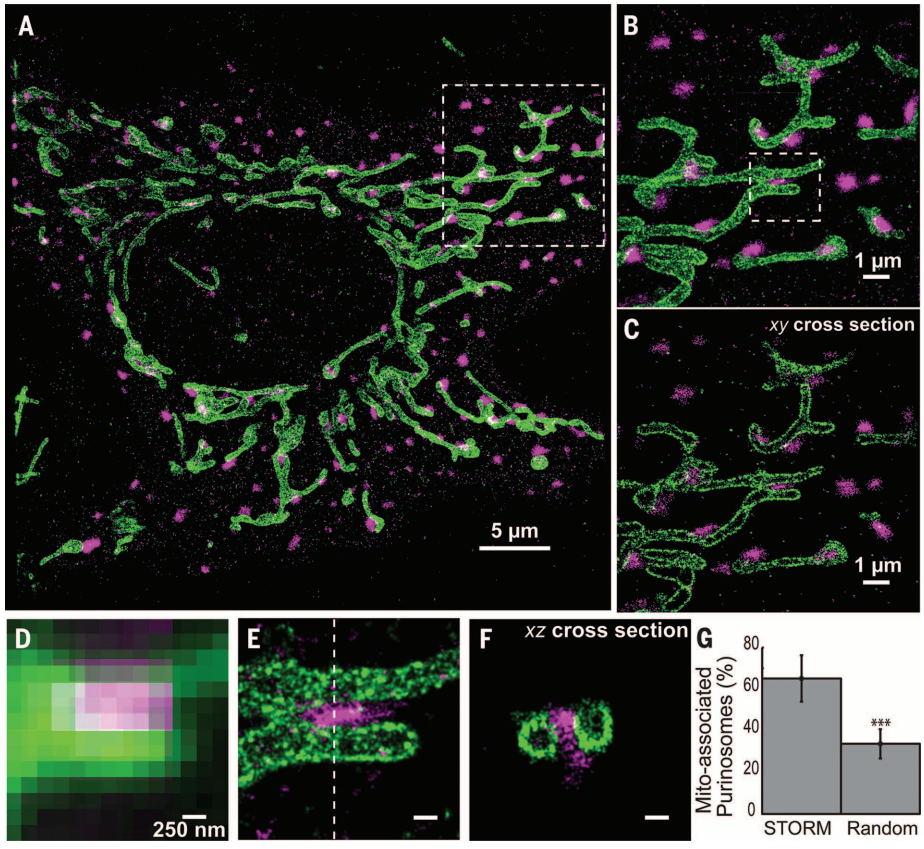

Fig. 1. Super-resolution imaging of purinosomes and mitochondria. (**A**) Two-dimensional projection of a 3D STORM image showing purinosomes labeled with mEos2 fused to a purinosome core protein FGAMS (magenta) and mitochondria immunolabeled against outer membrane protein TOM20 (green) in a HeLa cell grown under purine-depleted conditions. (**B**) Enlargement of the boxed region in (A) showing the close proximity between the two structures. (**C**) A 100-nm-thick *xy* cross section of the region in (B). (**D** and **E**) Comparison of the conventional fluorescence image (D) and corresponding 2D projection STORM image (E) of the boxed region in (B). (**F**) *xz* cross section along the dashed line in (E) showing a purinosome and two neighboring mitochondria. (**G**) The percentage of purinosomes (colocalized with mitochondria observed by STORM (65.1 ± 11.5%, mean ± SD) is significantly higher than the expected value for a randomized purinosome distribution (33.7 ± 7.3%). N = 26 images, Student's t test, $^{***}P << 0.001$. Scale bars (E and F): 250 nm.

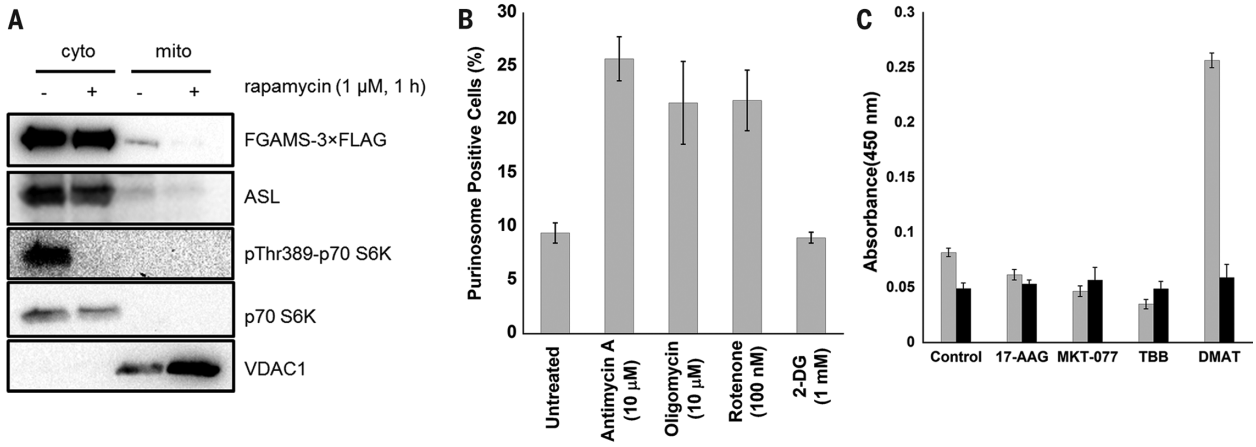

Fig. 2. Physical and functional links between purinosomes and mitochondria. (**A**) Western blot of purified mitochondria showing that purinosome proteins FGAMS and ASL co-isolate with mitochondria in a rapamycin-dependent manner. Mitochondria were isolated from HeLa cells grown under purine-depleted conditions that transiently expressed FGAMS-3×FLAG after treatment with 1 μM rapamycin (+) or vehicle control (-) for 1 hour. Inhibition of mTOR was verified by observing a decrease in the phosphorylated form (pT389) of the mTOR target S6 kinase (p70-S6K). VDAC1 was used as a mitochondria loading control, and p70-S6K served as a cytoplasmic loading control. (**B**) The percentage of cells with visible purinosomes (determined from at least 100 total cells) as a function of modulators of mitochondrial metabolism and glycolysis at their specified concentrations for 1 hour. Values reflect mean ± SD, N = 3 independent samples. (**C**) Intracellular malate (gray) and lactate (black) levels were determined by colorimetric assay after various drug treatments for 1 hour (2 hours for MKT-077). Values reflect mean ± SD, N = 3 independent samples.

to cytosolic fractions. Four different cross-linkers of varying length and reactivity were employed to minimize method bias, and the proteins that copurified with the mitochondria were identified by mass spectrometry (table S1). In addition to mitochondrial proteins such as ATP synthase, voltage-dependent anion channel, and malate dehydrogenase, one of the 174 proteins identified was adenylosuccinate lyase (ASL or ADSL), a known purinosome protein. ASL catalyzes the eighth step in de novo purine biosynthesis and was observed using three out of the four cross-linkers (table S1). To provide further evidence for ASL colocalization with mitochondria, we purified mitochondria from cells under purinosome-forming

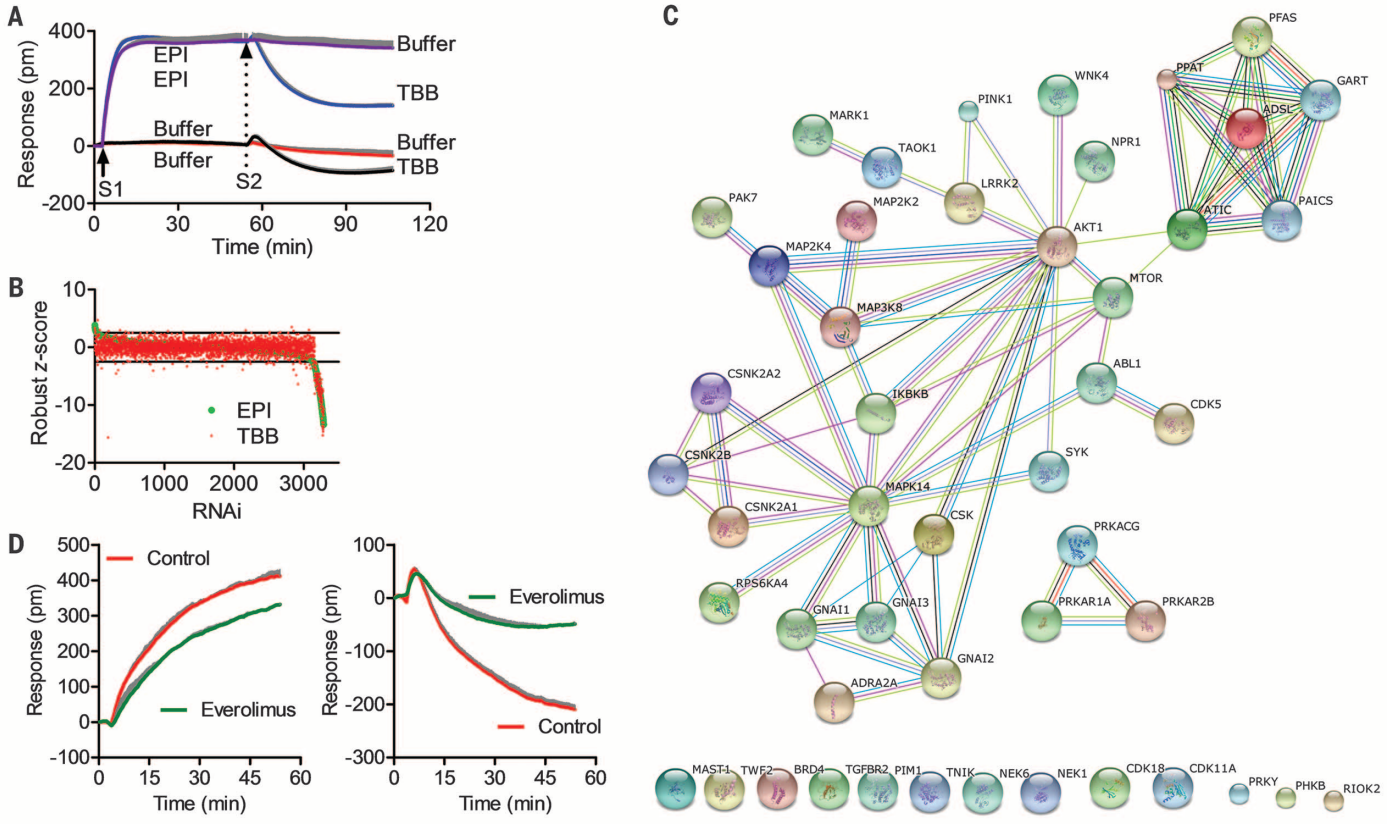

Fig. 3. Human kinome screen identified kinases involved in α_{2A}-adrenergic receptor (α_{2A}-AR) activation-mediated purinosome formation. (**A**) Characteristic DMR of HeLa cells in response to sequential stimulation steps (S1 and S2). Red line: buffer (S1)–buffer (S2); black line: buffer–TBB; purple line: EPI–buffer; blue line: EPI–TBB. The DMR of assay buffer stimulation was used as the negative control. Buffer by itself triggered little DMR and did not alter DMR induced by 100 nM epinephrine (EPI). EPI (100 nM) triggered a positive DMR. Conversely, TBB led to a negative DMR in the buffer-pretreated cells, but a much greater negative DMR in EPI-pretreated cells. (**B**) The robust *z* score of EPI-induced DMR (green dots) or TBB-induced DMR (red dots) as a function of shRNA clones. Robust *z* scores (a *z* score not adversely affected by outliers) were calculated using [(experimental data – median)/median absolute deviation (MAD)], where the normalization set the median to 0 and the MAD to 1. (**C**) Network analysis of the α_{2A}-AR activation-mediated purinosome formation. This analysis combines all hits common to the EPI and TBB DMR responses identified with the current kinome screen with known signaling components of endogenous α_{2A}-AR in HeLa cells, casein kinase 2 (CSNK2B, CSNK2A1, CSNK2A2), and six enzymes (PPAT, GART, PFAS, PAICS, ADSL, ATIC) involved in purine biosynthesis. Hits were selected when at least two shRNA clones for a kinase within the library gave a robust *z* score of ≥3 or ≤−3 (table S2). The network was generated with STRING 9.1. Connecting lines are color coded by the type of evidence used to build the network (details in http://string-db.org/). Unconnected hits are listed at the bottom. (**D**) (Left) The real-time DMR of EPI in the absence (red) or presence of everolimus (green). (Right) The real-time DMR of TBB after EPI prestimulation in the absence (red) or presence of everolimus (green). The dose was 16 μM, 100 nM, or 20 μM for everolimus, EPI, or TBB, respectively. For (A) and (D), data represent mean + SD, $N = 4$ (two independent measurements, each in duplicate). The standard deviation is shown in gray.

conditions without chemical cross-linking, and purinosome enzymes that copurified with mitochondria were detected by Western blot. In addition to ASL, FGAMS, a core protein of the purinosome structure, also coprecipitated with isolated mitochondria (Fig. 2A). Although these data demonstrate a physical link between purinosomes and mitochondria, further experiments are required to characterize the molecular details of this interaction and identify any structural intermediaries.

To investigate the functional relationship of purinosomes with mitochondria, we first examined the effect of mitochondrial poisons on purinosome content of cells. Inhibition of electron transport (using antimycin A or rotenone) or oxidative phosphorylation (using oligomycin) increased the number of purinosome-positive cells cultured in purine-rich conditions by more than twofold (Fig. 2B). Inhibition of glycolysis (using 2-deoxyglucose, 2-DG), which also lowers cellular ATP concentrations (*28*), had no effect on purinosome levels (Fig. 2B). The latter result, combined with previous observations of the effect of exogenous ATP treatments (*14*), suggests that although mitochondrial dysregulation induced a stimulation of purinosome formation in cells, the purinosome assembly is not governed by ATP concentration. Next, we examined the effect of purinosome levels on mitochondrial metabolism. As an approximate measure of glycolytic (cytosolic) and oxidative phosphorylation (mitochondrial) activities, we assayed cellular lactate and malate concentrations, respectively (*29*, *30*). Compounds known to disrupt or inhibit purinosome formation (17-AAG, MKT-077, and TBB) (*11*, *16*) led to decreases in malate levels, whereas an increase in purinosome content induced by DMAT (*11*) significantly increased malate production (Fig. 2C). Lactate levels were not changed by any of the purinosome effectors. These results indicate that there is also a functional link between purinosomes and mitochondria.

Previously, we reported that the assembly of purinosomes was stimulated by agonist binding to the α_{2A}-adenergic receptor and subsequent activation of the $G\alpha_i$-mediated signaling pathway (*14*). To identify the intracellular signaling pathway employed in the control of the relationship between purinosomes and mitochondria, we conducted a short hairpin RNA (shRNA) screen of the human kinome using a two-step dynamic mass redistribution (DMR) assay (Fig. 3A). DMR is a label-free method that uses a resonant waveguide grating biosensor system to

monitor, in real time, refractive-index alterations resulting from stimulus-induced biomass changes near the surface of a sensor (figs. S4 and S5) (*14*, *31*). Epinephrine (EPI) is known to induce purinosome assembly, which contributed to a DMR signal increase; TBB is known to cause purinosome disassembly, which contributed to a DMR signal decrease (*14*). Here we used the EPI-induced DMR signal as a purinosome assembly indicator and the EPI-stimulated TBB response as a purinosome disassembly indicator to identify kinases that influence purinosomes. Analyses of the robust *z* score (*32*) for each shRNA treatment (Fig. 3, A and B; fig. S6; and table S2) and Gene Ontology (GO) enrichment (table S3) suggest that some of the identified kinases are indeed associated with regulation of purine nucleotide metabolism. Using the STRING9.1 database that provides known and predicted protein-protein associations (*33*), we generated networks for the identified kinases that connect them to known components of endogenous α_{2A}-receptor signaling and purinosome assembly, including casein kinase 2 and the six enzymes of the de novo purine biosynthetic pathway (Fig. 3C and figs. S7 and S8). This analysis identifies a putative kinase network involved in directly translating chemical signals into a purinosome response.

Among the kinases identified in this screen were several known to be master regulators of cellular metabolism. Interestingly, one of these kinases was the mechanistic target of rapamycin (mTOR). mTOR, which actively associates with mitochondria-associated endoplasmic reticulum membranes and modulates mitochondrial physiology, is also involved in regulating nucleotide metabolism (*17*, *30*, *34*, *35*). Its role in modulating purine biosynthesis, however, is still unclear (*36*).

We examined the effect of mTOR inhibition on purinosome formation using the described DMR assay. Inhibition of mTOR with everolimus alone did not trigger a DMR response (fig. S9), but partially inhibited the EPI-induced DMR signal in a dose-dependent manner (Fig. 3D and fig. S9). The EPI-induced DMR signal contains contributions from the $G_{\alpha s}$ and $G_{\alpha i}$ pathways, the latter of which is related to purinosome formation (*6*, *14*). Moreover, mTOR inhibition also suppressed the EPI-potentiated TBB-induced DMR signal (Fig. 3D and fig. S9). Taken together, these results suggest a model wherein the inhibition of mTOR impairs α_{2A} receptor activation–stimulated purinosome formation.

To test whether mTOR plays a role in mediating the link between mitochondria and purinosomes, we monitored the observed stimulation of the cellular purinosome level in response to mitochondrial dysregulation. Although a large increase in the percentage of cells containing purinosomes was observed when mitochondrial function was disrupted by antimycin A, oligomycin, or rotenone, this response was abrogated by treatment with the mTOR inhibitor rapamycin (Fig. 4A), similar to the response observed with everolimus treatment of EPI-prestimulated cells (Fig. 3D). Rapamycin treatment alone had no effect on purinosome levels. Notably, the observations were made without purine deprivation or chemical stimulation of purinosome levels, where such an effect would be difficult to detect. We then examined the colocalization between mitochondria and purinosomes, under conditions of purine depletion, in the presence of rapamycin using two-color STORM. Indeed, fractional colocalization between purinosomes and mitochondria decreased in a dose-dependent manner with increasing concentration of rapamycin (Fig. 4B), whereas both the number and size of purinosomes and the cellular distributions of mitochondria were unchanged up to concentrations of 100 nM or higher (fig. S10). Finally, to further show that mTOR plays a role in mediating a physical link between purinosomes and mitochondria, we probed for the presence of FGAMS and ASL in isolated mitochondria from cells treated with rapamycin (Fig. 2A). Although these purinosome markers were observed in the mitochondrial fraction in the absence of rapamycin, they were either not observed or observed at a substantially reduced level in rapamycin-treated cells. Taken together, these data suggest that mTOR plays a role in the link between purinosomes and mitochondria.

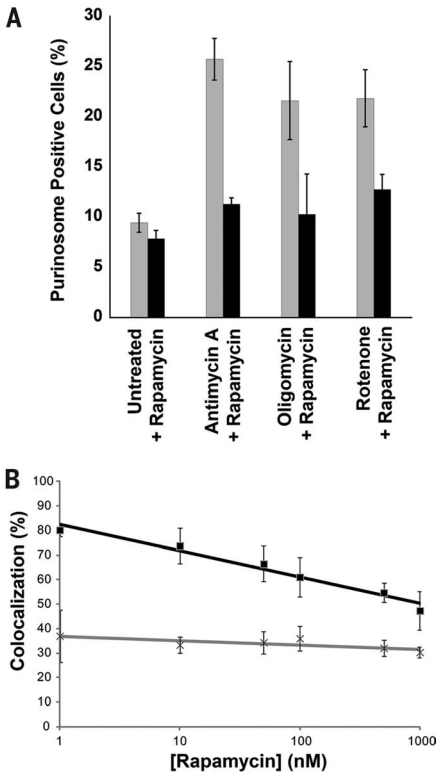

Fig. 4. mTOR affects colocalization and functional links between purinosomes and mitochondria. (**A**) The percentage of purinosome-containing cells (determined from at least 100 cells) as a function of mitochondrial metabolism modulators in the absence (gray) and presence (black) of 100 nM rapamycin. Values reflect the mean ± SD, $N = 3$ independent samples. (**B**) The percentage of purinosomes colocalized with mitochondria (black squares) in STORM images of HeLa cells grown under purine-depleted conditions as a function of increasing rapamycin concentration (10 to 1000 nM, 1 hour). The results after randomization of the purinosome distribution are shown as gray crosses. The colocalization percentage is represented as the mean ± SD, $N = 5$ images per condition.

Two recent reports detailed the mTOR-mediated stimulation of pyrimidine synthesis (*17*, *34*). The mechanism of control exerted by mTOR on pyrimidine metabolism—the change in oligomerization and localization of the enzyme CAD—mirrors the observed effects reported here. Pyrimidine biosynthesis also uses a mitochondrial enzyme, dihydroorotate dehydrogenase, further evidence for the relationship between nucleotide metabolism and the mitochondria. mTOR nucleates into two distinct multiprotein complexes (mTORC1 and mTORC2) and is known to regulate protein associations to control other cellular processes, such as autophagy (*37*–*39*).

The maintenance of nucleotide pools and the rapid response to changing levels of these critical building blocks are vital cellular processes. Management of metabolite levels in a dynamic microenvironment necessitates highly regulated posttranslational control over metabolic flux. This study suggests a spatial mechanism of control. The mTOR-mediated link between purinosomes and mitochondria creates a functional synergy and highlights the interdependence between mitochondrial function and nucleotide metabolism, which could provide a controllable response to changes in metabolic needs. This type of regulation is only beginning to be understood but is likely to emerge as a common mechanism by which cells exploit spatial and temporal control of enzymes and enzyme complexes to increase metabolic efficiency, protect unstable intermediates, and minimize off-target effects.

REFERENCES AND NOTES

1. T. Yamaoka *et al.*, *J. Biol. Chem.* **272**, 17719–17725 (1997).
2. T. Yamaoka *et al.*, *J. Biol. Chem.* **276**, 21285–21291 (2001).
3. L. Antonioli, C. Blandizzi, P. Pacher, G. Haskó, *Nat. Rev. Cancer* **13**, 842–857 (2013).
4. Y. Natsumeda, N. Prajda, J. P. Donohue, J. L. Glover, G. Weber, *Cancer Res.* **44**, 2475–2479 (1984).
5. S. An, R. Kumar, E. D. Sheets, S. J. Benkovic, *Science* **320**, 103–106 (2008).

6. H. Zhao, J. B. French, Y. Fang, S. J. Benkovic, *Chem. Commun. (Camb.)* **49**, 4444–4452 (2013).
7. P. C. Havugimana *et al.*, *Cell* **150**, 1068–1081 (2012).
8. F. J. Schendel, Y. S. Cheng, J. D. Otvos, S. Wehrli, J. Stubbe, *Biochemistry* **27**, 2614–2623 (1988).
9. Q. C. Zhang *et al.*, *Nature* **490**, 556–560 (2012).
10. H. Zhao *et al.*, *J. Biol. Chem.* **290**, 6705–6713 (2015).
11. S. An, M. Kyoung, J. J. Allen, K. M. Shokat, S. J. Benkovic, *J. Biol. Chem.* **285**, 11093–11099 (2010).
12. C. Y. Chan *et al.*, *Proc. Natl. Acad. Sci. U.S.A.* **112**, 1368–1373 (2015).
13. Y. Fang, J. French, H. Zhao, S. Benkovic, *Biotechnol. Genet. Eng. Rev.* **29**, 31–48 (2013).
14. F. Verrier *et al.*, *Nat. Chem. Biol.* **7**, 909–915 (2011).
15. R. Fu *et al.*, *Mol. Genet. Metab.* **114**, 55–61 (2015).
16. J. B. French *et al.*, *Proc. Natl. Acad. Sci. U.S.A.* **110**, 2528–2533 (2013).
17. A. M. Robitaille *et al.*, *Science* **339**, 1320–1323 (2013).
18. F. M. Meyer *et al.*, *Metab. Eng.* **13**, 18–27 (2011).
19. P. D. Straight, M. A. Fischbach, C. T. Walsh, D. Z. Rudner, R. Kolter, *Proc. Natl. Acad. Sci. U.S.A.* **104**, 305–310 (2007).
20. C. Jose, N. Bellance, R. Rossignol, *Biochim. Biophys. Acta* **1807**, 552–561 (2011).
21. L. J. Reitzer, B. M. Wice, D. Kennell, *J. Biol. Chem.* **254**, 2669–2676 (1979).
22. B. Huang, S. A. Jones, B. Brandenburg, X. Zhuang, *Nat. Methods* **5**, 1047–1052 (2008).
23. B. Huang, W. Wang, M. Bates, X. Zhuang, *Science* **319**, 810–813 (2008).
24. M. J. Rust, M. Bates, X. Zhuang, *Nat. Methods* **3**, 793–796 (2006).
25. S. A. McKinney, C. S. Murphy, K. L. Hazelwood, M. W. Davidson, L. L. Looger, *Nat. Methods* **6**, 131–133 (2009).
26. Y. Deng *et al.*, *J. Biol. Chem.* **287**, 36201–36207 (2012).
27. S. Wang, J. R. Moffitt, G. T. Dempsey, X. S. Xie, X. Zhuang, *Proc. Natl. Acad. Sci. U.S.A.* **111**, 8452–8457 (2014).
28. H. Pelicano, D. S. Martin, R. H. Xu, P. Huang, *Oncogene* **25**, 4633–4646 (2006).
29. N. Masson, P. J. Ratcliffe, *Cancer Metab.* **2**, 3 (2014).
30. A. Ramanathan, S. L. Schreiber, *Proc. Natl. Acad. Sci. U.S.A.* **106**, 22229–22232 (2009).
31. Y. Fang, *Front. Pharmacol.* **5**, 52 (2014).
32. A. Birmingham *et al.*, *Nat. Methods* **6**, 569–575 (2009).
33. A. Franceschini *et al.*, *Nucleic Acids Res.* **41** (D1), D808–D815 (2013).
34. I. Ben-Sahra, J. J. Howell, J. M. Asara, B. D. Manning, *Science* **339**, 1323–1328 (2013).
35. K. Düvel *et al.*, *Mol. Cell* **39**, 171–183 (2010).
36. M. Shimobayashi, M. N. Hall, *Nat. Rev. Mol. Cell Biol.* **15**, 155–162 (2014).
37. I. G. Ganley *et al.*, *J. Biol. Chem.* **284**, 12297–12305 (2009).
38. C. H. Jung *et al.*, *Mol. Biol. Cell* **20**, 1992–2003 (2009).
39. M. Laplante, D. M. Sabatini, *J. Cell Sci.* **122**, 3589–3594 (2009).

ACKNOWLEDGMENTS

We thank T. Laremore at the Proteomics and Mass Spectrometry Core Facility of the Huck Institutes of the Life Sciences at The Pennsylvania State University for assistance with data collection and analyses. The Orbitrap mass spectrometer was funded by a grant from the Pennsylvania Department of Health Tobacco Settlement Funds. J.B.F. acknowledges the Canadian Institutes of Health Research for fellowship support. This work was funded by the National Institutes of Health grants NIH GM024129 (S.J.B.) and 1R33EB019785-01 (T.J.H. and S.J.B.) as well as the Howard Hughes Medical Institute (X.Z.). J.B.F., S.A.J., Y.F., X.Z., and S.J.B. designed the experiments; J.B.F., S.A.J., H.D., H.H., A.M.P., C.Y.C., D.K., R.J.P., H.Z., and Y.Z. performed the experiments and analyzed the data; J.B.F., S.A.J., A.M.P., R.J.P., and Y.F. prepared the manuscript; J.B.F., Y.F., X.Z., and S.J.B. directed the research; all authors have reviewed and edited the manuscript. The authors declare that they have no competing interests. Additional data reported in this manuscript are available in the supplementary materials.

SUPPLEMENTARY MATERIALS

www.sciencemag.org/content/351/6274/733/suppl/DC1
Materials and Methods
Figs. S1 to S10
Tables S1 to S3

19 May 2015; accepted 23 December 2015
10.1126/science.aac6054

HUMAN GENOMICS

The phenotypic legacy of admixture between modern humans and Neandertals

Corinne N. Simonti,[1] Benjamin Vernot,[2] Lisa Bastarache,[3] Erwin Bottinger,[4] David S. Carrell,[5] Rex L. Chisholm,[6] David R. Crosslin,[2,5] Scott J. Hebbring,[7] Gail P. Jarvik,[2,5] Iftikhar J. Kullo,[8] Rongling Li,[9] Jyotishman Pathak,[10]* Marylyn D. Ritchie,[11,12] Dan M. Roden,[1,3,13,14] Shefali S. Verma,[11] Gerard Tromp,[15,16] Jeffrey D. Prato,[3] William S. Bush,[17] Joshua M. Akey,[2]† Joshua C. Denny,[1,3,13]† John A. Capra[1,3,18,19]‡

Many modern human genomes retain DNA inherited from interbreeding with archaic hominins, such as Neandertals, yet the influence of this admixture on human traits is largely unknown. We analyzed the contribution of common Neandertal variants to over 1000 electronic health record (EHR)–derived phenotypes in ~28,000 adults of European ancestry. We discovered and replicated associations of Neandertal alleles with neurological, psychiatric, immunological, and dermatological phenotypes. Neandertal alleles together explained a significant fraction of the variation in risk for depression and skin lesions resulting from sun exposure (actinic keratosis), and individual Neandertal alleles were significantly associated with specific human phenotypes, including hypercoagulation and tobacco use. Our results establish that archaic admixture influences disease risk in modern humans, provide hypotheses about the effects of hundreds of Neandertal haplotypes, and demonstrate the utility of EHR data in evolutionary analyses.

As anatomically modern human (AMH) groups left Africa and began to spread across Europe and Asia ~60,000 years ago, they encountered other archaic hominins. The fossil record suggests that AMHs and several archaic hominins overlapped in space and time (*1*), and genomic analyses of modern and ancient humans and of extinct Neandertals and Denisovans have revealed interbreeding between these groups (*2*, *3*). As a result, the genomes of modern Eurasians contain a small fraction (~1.5 to 4%) of DNA inherited from interbreeding with Neandertals around 50,000 years ago (*4*–*6*).

The patterns of surviving Neandertal DNA across modern Eurasian genomes indicate that introgressed Neandertal DNA experienced strong selective pressures. Surviving Neandertal lineages are significantly depleted in several genomic regions, such as on the X chromosome and the q arm of chromosome 7, suggesting that there are deleterious consequences of Neandertal DNA at many loci (*5*, *6*). However, some Neandertal alleles are found at higher than expected frequencies and thus may have provided an evolutionary advantage to AMH populations (*5*–*7*). Consistent with this hypothesis, Neandertals are believed to have lived out of Africa long enough to adapt to the climatic, dietary, and pathogenic landscapes found at higher latitudes.

Indeed, isolated introgressed loci have been identified with potential roles in human adaptation (*7*, *8*). Furthermore, recent studies of genomic regions enriched in Neandertal alleles have suggested potential effects on skin and hair phenotypes, lipid metabolism, depression, and other traits (*5*, *6*, *9*). However, whether introgressed Neandertal alleles have a significant functional effect on these traits in human populations has

[1]Vanderbilt Genetics Institute, Vanderbilt University, Nashville, TN, USA. [2]Department of Genome Sciences, University of Washington, Seattle, WA, USA. [3]Department of Biomedical Informatics, Vanderbilt University, Nashville, TN, USA. [4]Mount Sinai School of Medicine, New York, NY, USA. [5]Department of Medicine (Medical Genetics), University of Washington Medical Center, Seattle, WA, USA. [6]Center for Genetic Medicine, Feinberg School of Medicine, Northwestern University, Chicago, IL, USA. [7]Center for Human Genetics, Marshfield Clinic, Marshfield, WI, USA. [8]Division of Cardiovascular Diseases, Mayo Clinic, Rochester, MN, USA. [9]Division of Genomic Medicine, National Human Genome Research Institute, National Institutes of Health, Bethesda, MD, USA. [10]Division of Health Sciences Research, Mayo Clinic, Rochester, MN, USA. [11]Department of Biochemistry and Molecular Biology, The Pennsylvania State University, University Park, PA, USA. [12]Biomedical and Translational Informatics, Geisinger Health System, Danville, PA, USA. [13]Department of Medicine, Vanderbilt University, Nashville, TN, USA. [14]Department of Pharmacology, Vanderbilt University, Nashville, TN, USA. [15]Weis Center for Research, Geisinger Health System, Danville, PA, USA. [16]Division of Molecular Biology and Human Genetics, Department of Biomedical Sciences, Faculty of Health Science, Stellenbosch University, Tygerberg, South Africa. [17]Department of Epidemiology and Biostatistics, Case Western Reserve University, Cleveland, OH, USA. [18]Department of Biological Sciences, Vanderbilt University, Nashville, TN, USA. [19]Center for Quantitative Sciences, Vanderbilt University, Nashville, TN, USA.
*Department of Healthcare Policy and Research, Weill Cornell Medical College, New York, NY, USA. †These authors contributed equally to this work. ‡**Corresponding author. E-mail: tony.capra@vanderbilt.edu**

Spatial colocalization and functional link of purinosomes with mitochondria

Jarrod B. French *et al.*

Science **351**, 733 (2016);
DOI: 10.1126/science.aac6054

Science (print ISSN 0036-8075; online ISSN 1095-9203) is published weekly, except the last week in December, by the American Association for the Advancement of Science, 1200 New York Avenue NW, Washington, DC 20005.